5.2 Linear-perturbation Models Applied to Vegetation Covered Terrain

The linear-perturbation analysis approach originates with Townsend's (1966) analysis of roughness changes and the inviscid and laminar flow theories of perturbed shear flow and stratified flow. Jackson and Hunt (1975) developed algebraic equations which predicted the development of wind and turbulence over moderate slope two-dimensional hills and ridges. The advantage of the linear theory is that it enables formulae for the flow to be derived analytically. Independent effects of elevation variation, roughness, surface temperature variation, and atmospheric stratification are superimposed through addition of the individual perturbations calculated for each effect. Of course linear theories *cannot* describe large nonlinear-perturbations to the flow or nonlinear interactions where two or more effects combine such as roughness change and flow separation. Subsequently, it was recognized that if the surface elevations in arbitrary terrain were converted through Fourier transform into its component waves perturbation solutions could be obtained to the individual waves, and the resultant velocities can be re-transformed and summed into actual flow velocities (Carrruthers and Hunt, 1990). In contrast to numerical models that solve the equations of motion on a grid, there is no iteration involved and no doubt about the solution once the algorithms and their assumptions have been established. The resultant program is quite appropriate for use on small personal computers. The conditions on terrain and meteorology which must be satisfied for realistic solutions are mentioned in Appendix Section 3.0. Table A.2 lists several linear-perturbation models suitable for wind energy analysis.

5.2.1 *FLOWSTAR Model Predictions*

FLOWSTAR is designed to predict velocity fields over complex terrain in the presence of elevation variation, roughness variation, and stratification. The program is packaged with post processing graphics that can produce a streamline, flow vector, or profile graphs. The program is commercially distributed by Cambridge Environmental Research Consultants, Cambridge, U.K. Carruthers and Hunt (1990) report examples of output of the model applied to flow over isolated hills Brent Knoll and Great Dun Fell in England. No public literature references were found for the application of the program to forested terrain, and most subsequent publications relate to using the program to provide velocity fields to predict pollutant dispersion or the modification of temperature and humidity fields.

5.2.2 *MS3DJH and MS-MICRO Model Predictions*

The MS3DJH series of models are primarily intended to predict neutrally stratified wind flows over surfaces with variations of elevation and surface roughness. The model predicts velocities on one surface plain at a time. The wind data can then be exported for evaluation on commercial graphics software such as SURFER. A PC-version of MS3DJH designated MS-MICRO has also been coded. The programs are available at nominal cost directly from the Atmospheric Environment Service, Canada.

Walmsley, Taylor and Keith (1986) considered sinusoidal variations of roughness, predicted their influence with the MS3DJH program, and compared them to finite difference solutions over the same roughness variations. At values of $\lambda/z_o < 10^3$ phase errors appeared in the surface shear distribution probably due to advection errors. Also under the same limitations the lower level perturbation velocities were under predicted **(Figures 5.2.1 and 5.2.2)** . The model dealt with the step change in roughness problem quite well.. A series of 2-dimensional idealized terrain cases were examined with surface roughness variations. Gaussian shape hills were specified and both rough approach surfaces with smooth hills and smooth approach surfaces with rough hills were considered. Test cases were calculated for $h_{hill} = 100$ m, $\beta = 500$ m, $z_{ou} = 0.01$ m and $z_{0d} = 0.1$ m at the crest. for the rough-crested hill. The opposite roughness sequence was specified for the smooth crested hill. **Table 5.2.1** summarizes the predictions of MS3DJH and a finite difference model. The model appears to perform rather better with roughness or topography alone and tends to underestimate the surface stress perturbations at the crest in the combined case, **Figures 5.2.3, 5.2.4, and 5.2.5**. The neglect of nonlinear interactions must be partially responsible for this. The lee regions where non-linear effects become important are not predicted as well as the crest and upwind parts of the hill.

Finally two 3-D idealized hills with and without roughness were studied: (i) a 'Coastal Hill', an idealized circular coastal hill of cosine-squared section and (ii) an 'Island', a rough-crested cosine-squared hill with a cosine-squared distribution of $\ln[z_o]$. **Figure 5.2.6** shows cross-sections of normalized with speed (S/u_o) along the x-axis at $z = 2$ m. The contribution of the roughness change alone are quite different between the two experiments. When elevation effects are added, the shapes of the curves in the two cases appear similar, although the wind recovers to within 97% of the upwind values in the Coastal Island case. **Figure 5.2.7** illustrates the normalized wind speed at the crest of the hill. Above $z = 20$ m, the differences between the two cases are small. At lower levels the different roughness patterns produce larger velocities over the Coastal Island.

Walmsley and Taylor (1987) proposed to use the AES Regional Finite element Model (EFR) to predict areal averaged winds over 100 km squares. Then within a 256 square km region with a 128 square km central region finely represented the MS3DJH model could be used to interpolate the EFR data. Subsequently, a second interpolation could be made for a 15 square km region within which an 8 square km area can be finely represented for terrain as well as roughness variation. Demonstration runs were provided for several areas in Nova Scotia, Canada where meteorological observations were available for comparison. Land cover is mostly pine forest ($z_o = 1$ m), but main valley areas are cleared for farming ($z_o = 0.05$ m). The calculated wind velocities predicted up to 50% variations over high resolution areas. An algorithm was proposed to combine the various predictions into a forecast wind:

$$U(z = 10 \text{ m}) = U_R(10) S_{II} S(x,y),$$

where $U_R(10)$ = forecast FEM wind speed as average of 9 values at a 10 m height,
S_{II} = is normalized average of nine values in coarse resolution model, and
$S(x,y)$ = is the prediction from the fine resolution run.

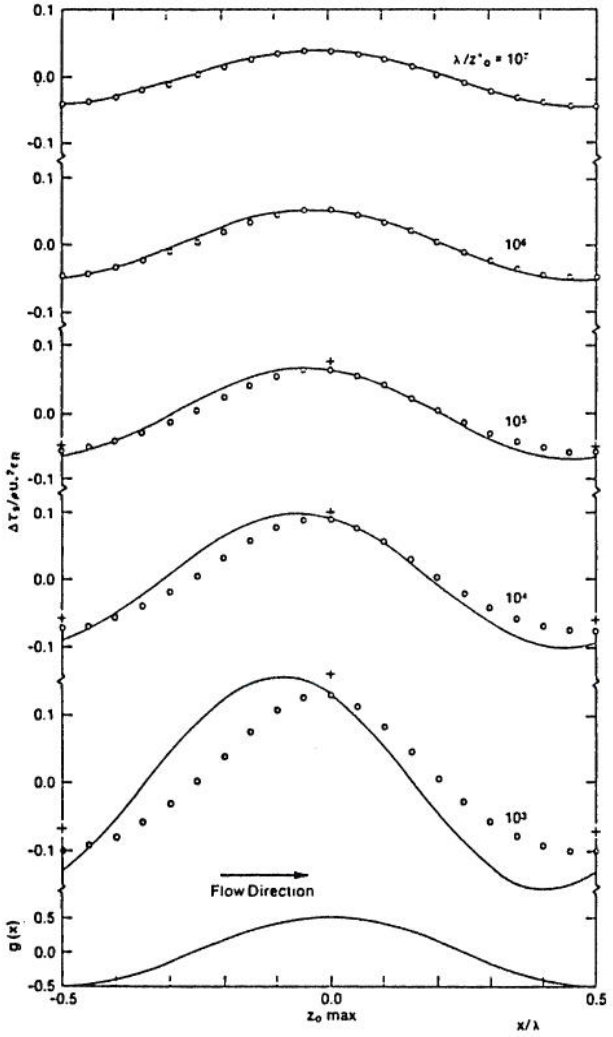

Figure 5.2.1 Sinusoidal hill & ln{z_o}.——— MS3DJH/3R, finite diff. model, m_r = 4; + , m_r = 100. (Walmsley *et al.* 1987)

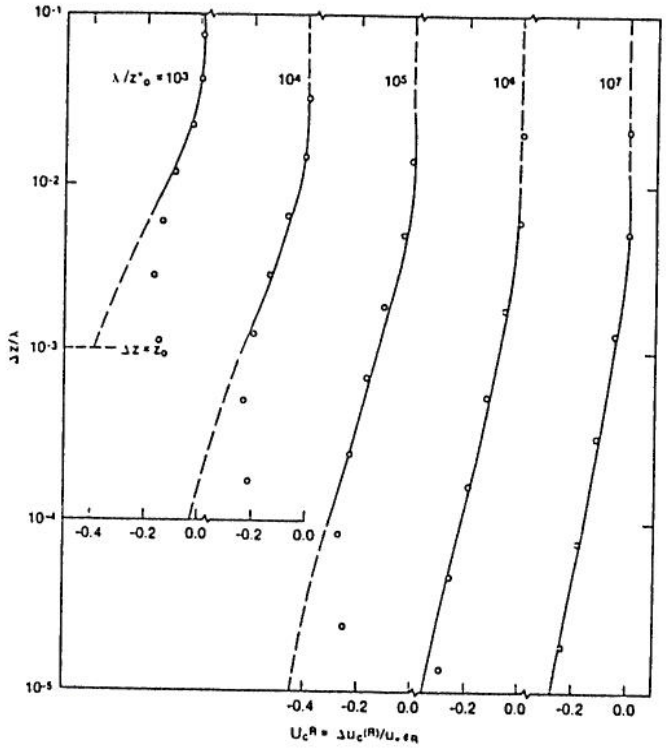

Figure 5.2.2 Crest velocities for sinusoidal hill and ln[z_o], ———MS3DJH/3R; Finite diff. m_r= 4. (Walmsley *et al.*, 1986)

Table 5.2.1 MS3DJH/3R and finite-difference model predictions for flow over Gaussian hills with roughness modulation. (Walmsley *et al.*, 1986)

MS3DJH/3R and finite-difference model predictions for flow over Gaussian hills with roughness modulation.

Terrain $z_s = h \exp[-(x/\beta)^2]$: $h = 100$ m, $2\beta = 1000$ m.
Domain length $XR = 12.8$ km for MS3DJH/3R computations. Underlined values indicate the choices of z_0^* giving best agreement with the finite-difference model at $\Delta z = 10$ m.

(i) Rough-crested hill
$\ln(z_0/z_{0u}) = M \exp[-(x/\beta)^2]$: $z_{0u} = 0.01$ m, $M = \ln 10$ ($m_r = 10$)

	Surface pressure $p_c/\rho u_*^2$	Velocity perturbation, $\Delta u/u_*$ at $x = 0$								
		$\Delta z = 1$ m			$\Delta z = 10$ m			$\Delta z = 100$ m		
		(1)	(2)	(3)	(1)	(2)	(3)	(1)	(2)	(3)
MS3DJH/3R										
(a)	−117	5.19	−2.08	3.11	6.88	−0.51	6.37	4.59	+0.01	4.60
(b)	−117	4.67	−2.48	2.19	6.79	−0.63	6.17	4.59	+0.01	4.60
(c)	−117	3.96	−3.02	0.94	6.65	−0.80	5.85	4.59	+0.01	4.61
Finite-difference model (1)	−142	4.62	−3.12	−0.35	6.86	−0.97	5.16	4.76	+0.01	4.75
(3)	−141									

(a) $z_0^* = 0.01$ m (upstream value).
(b) $z_0^* = 0.03162$ m.
(c) $z_0^* = 0.1$ m (crest value).
(1) Topography only.
(2) Roughness modulation only.
(3) Topography plus roughness modulation.

(ii) Smooth-crested hill
$\ln(z_0/z_{0u}) = -M \exp[-(x/\beta)^2]$: $z_{0u} = 0.1$ m, $M = \ln 10$ ($m_r = 10$)

	Surface pressure $p_c/\rho u_*^2$	Velocity perturbation, $\Delta u/u_*$ at $x = 0$								
		$\Delta z = 1$ m			$\Delta z = 10$ m			$\Delta z = 100$ m		
		(1)	(2)	(3)	(1)	(2)	(3)	(1)	(2)	(3)
MS3DJH/3R										
(a)	−65.5	2.99	3.19	6.18	5.22	1.01	6.23	3.98	−0.01	3.97
(b)	−65.5	4.00	2.24	6.24	5.48	0.68	6.16	3.97	−0.01	3.96
Finite-difference model (1)	−80.5									
(3)	−79.3	2.10	2.24	5.97	4.75	0.76	6.24	3.75	0.02	3.80

(a) $z_0^* = 0.1$ m (upstream value).
(b) $z_0^* = 0.01$ m (crest value).
(1) Topography only ($z_0 = 0.1$ m).
(2) Roughness modulation only.
(3) Topography plus roughness modulation.

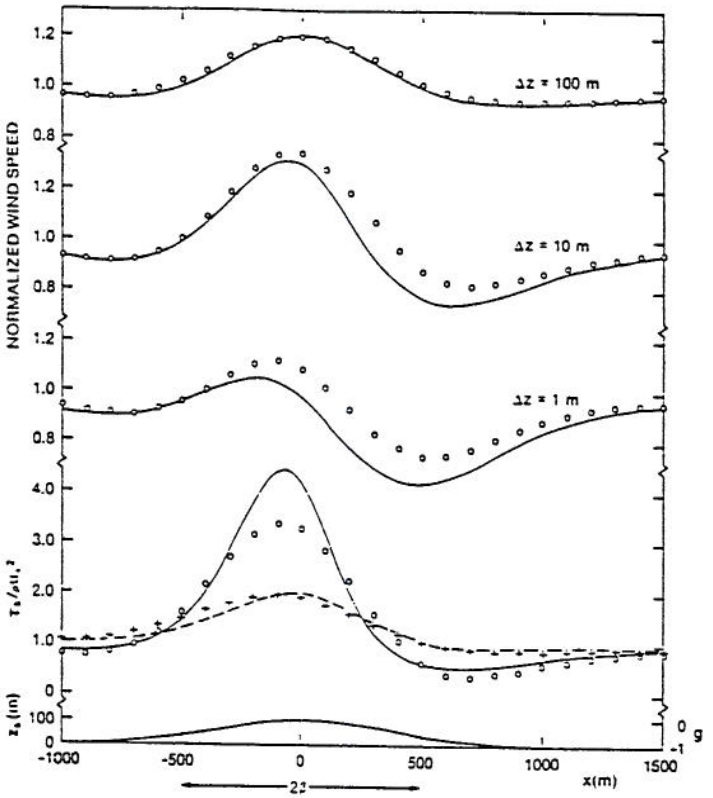

Figure 5.2.3 Rough-crested 2-D Gaussian hill,(2β=1000m, h=100m, m_r=10)———u,--- roughness only fd model;◯, + roughness only MS3DJH/3R model,

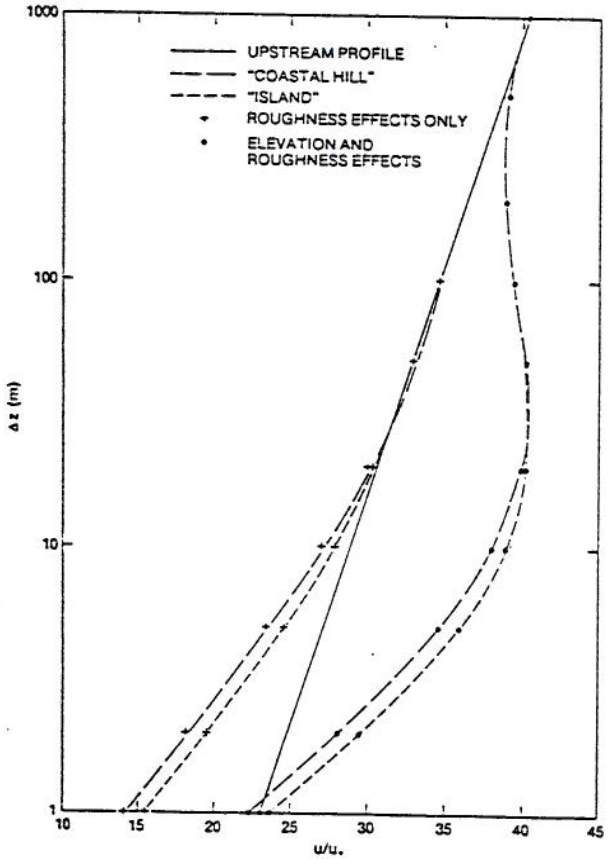

Figure 5.2.4 Crest velocities over rough-crested 2-D Gaussian hill (See Figure 5.2.3 for notation) (Walmsley *et al.*, 1986)

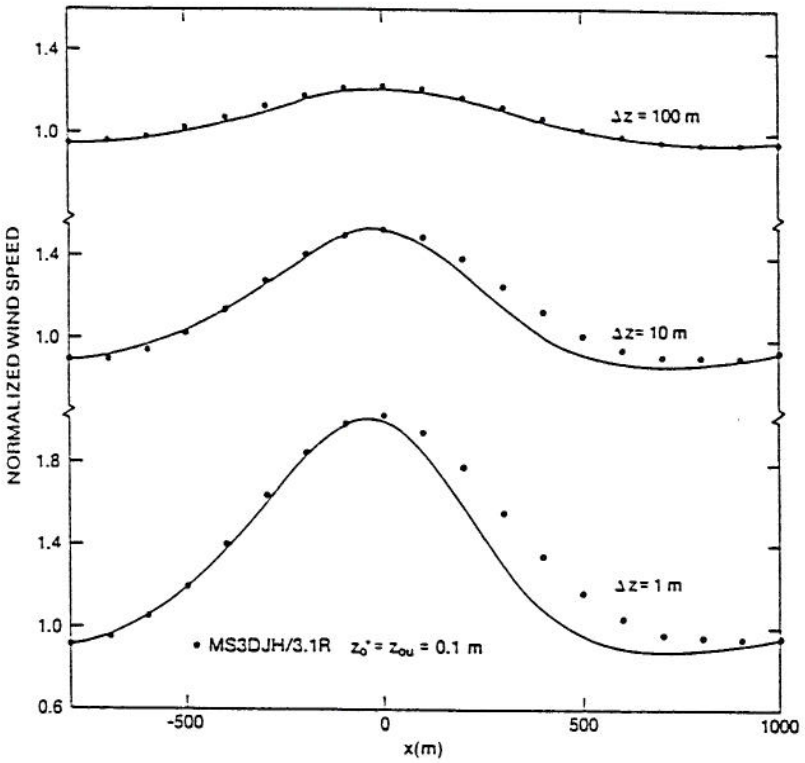

Figure 5.2.6 Wind speed at z = 2m for Coastal and Island experiments. Dashed curves are roughness change alone. (Walmsley *et al.*, 1986)

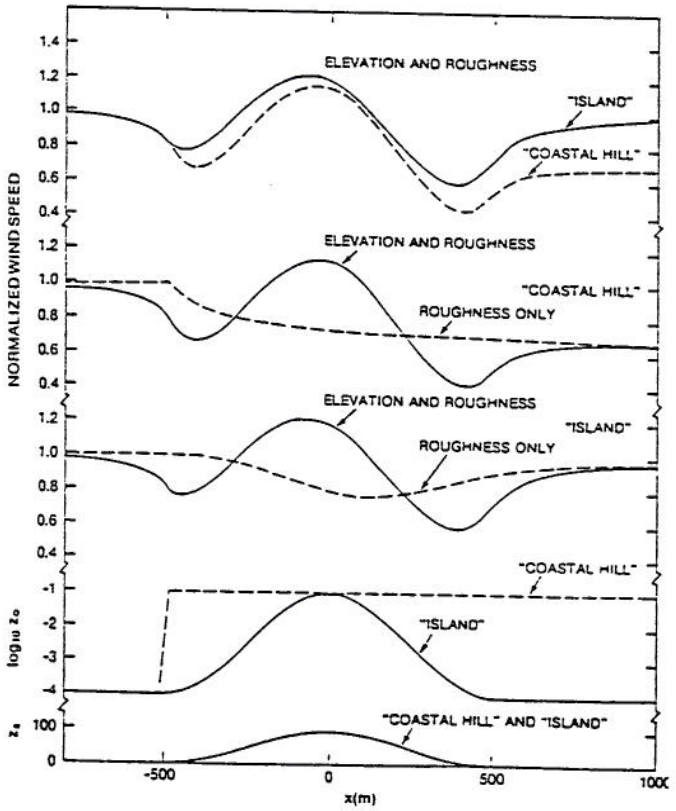

Figure 5.2.7 Cresttop velocities for the Coastal Hill and Island experiments. (Walmsley *et al.*, 1986)

For one case tested a 1 hr forecast of wind speed resulted in U(10) = 13.0 m/s but the actual observed average was 8.4 m/s. But corrections in roughness specified in the S_{II} level model to allow for roughness over the nearby ocean produced a revised estimate U(10) = 9.2 m/s. .

5.2.3 *Mass-consistent and Linear-perturbation Model Comparisons*

Lalas, Tombrou and Petrakis (1988) ran three numerical codes for wind-energy siting, WAsP of the Danish National Laboratory, MS-MICRO of the Atmospheric Environment Service of Canada, and NOABL* of Science Application Inc. for two sites on Limnos, an island in the norther Aegean sea with strong topography. WAsP and MS-MICRO are both based on linear-perturbation concepts. NOBAL* is a modified mass-consistent algorithm which includes initialization by logarithmic velocity profiles, the specification of different surface roughness at grid point, and variable transmissivity coefficient in the vertical direction.

Since most previous comparisons looked at hills that were rather isolated and simply shaped the intent of this study was to compare results in a more complex (and more realistic) environment. The island of Limnos has hills rising to 420 m and wind data have been taken at five sites on the island for some years. Three sites were selected for numerical simulation, two are in relatively smooth terrain and the third in a hillier region. **Figure 5.2.8** displays the winds predicted at the hilly site by the three codes. The mass-consistent model NOABL* was easy enough to use, but it took more computer resources and generally under-predicted wind speeds. WAsP produced the best combination of accuracy, ease of operation and computing power requirements. The version of MS-MICRO available was not easy to use and overpredicted wind speeds.

5.3 Primitive Equation Models Applied to Vegetation Covered Terrain

Primitive equation models compute all meteorological variables directly given appropriate initial and boundary conditions. The model codes can vary widely depending upon discretization, turbulence closure, initialization, and solution algorithms (FDM, FEM, FVM, etc.). Appendix Section 3.0 summarizes some features of such codes, and Appendix Table A.3 documents some of the major primitive equation codes. Because of the grid sizes generally treated in meso-scale models, the details of local or under-forest canopy flows are not always resolved. Since forest features are typically sub-grid scale their presence are accounted for by incorporation of appropriate drag terms.

5.3.1 *HOTMAC Predictions of Forest and Vegetation Effects*

Yamada (1982) used a simplified second-moment turbulence closure model to calculate the effects of a homogeneous infinite extent tree canopy on surface fluxes, wind speeds and turbulence. Yamada stipulated the normal 2.5-turbulence closure model that solves turbulent kinetic energy and length scale transport equations; however, terms were added in mean motion equations, turbulence energy equations, and length-scale equations for a form drag associated with the trees.

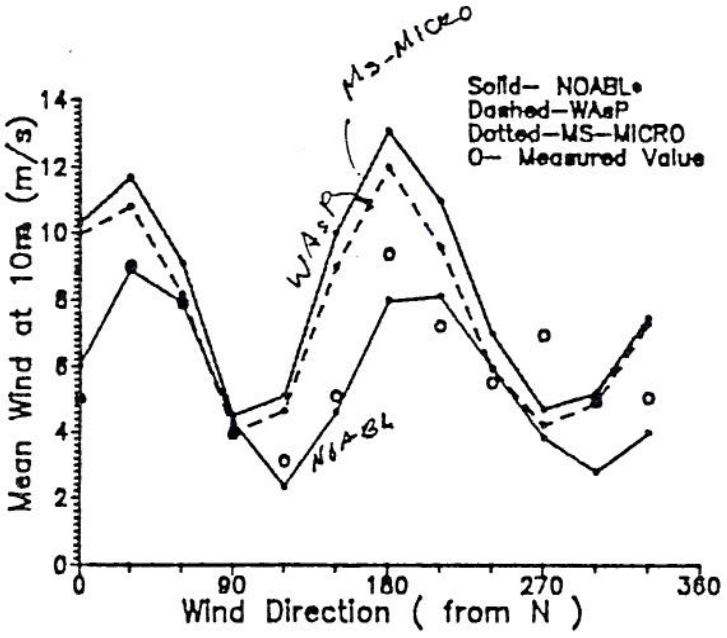

Figure 5.2.8 Mean wind speeds for each of 12 directions computed by WAsP, NOABL*, and MS-MICRO and measured values at Vounaros. (Lalas *et al.*, 1988)

The approach is based on idea that:

$$dp/dx = C_d a(z)\, U_i\, |U_i|,$$

where C_d is drag coefficient, a(z) is the plant area density, and the absolute sign insures that the direction of the drag force is always opposite to the wind direction. Corrections to the thermal energy equation were also proposed to adjust for radiation absorption and emission from the vegetation. Yamada calculated diurnal variation of potential temperatures, wind speeds, kinetic energy, eddy viscosity, and length scale for various assumed levels of vegetation coverage. As expected trees slow down the wind near the surface significantly.

Yamada and Bunker (1989) incorporated the tested drag and radiation relations into a three-dimensional mesoscale model HOTMAC. They applied this model with its vegetation adjustments to predict nocturnal drainage flows which develop during the evening in the Brush Creek valley in Colorado. Nudging was used to follow flow above the ridge top from observed (ASCOT 1984 field program) wind directions. Deviations from horizontally averaged temperatures and wind speeds were computed. **Figure 5.3.1** displays the horizontal distribution of tree canopies in the nested grid, and **Figure 5.3.2** shows typical horizontal wind vectors at 24 m above the ground a about 2 a.m. The tall tree canopy was believed to explain the inhomogeneous wind distributions, especially in levels below the canopy top. Notice that down valley flow vectors are reduced in forested regions.

5.3.2 *FITNAH Vegetation Modifications to Predict Deforestation Effects on Drainage Flows and Local Climate*

Gross (1987) modified a 3-d mesoscale model FITNAH to include the effects of a tall tree canopy on airflow in complex terrain. Specifically he examined a nighttime situation for cases with and without a canopy. He found surface wind speed will increase after deforestation. Tree effects were included by using the distributed drag system suggested by Yamada (1982). Terrain following coordinates were introduced such that $\eta = (z-h)/(H-h)$, where h is the height of the topography and H is the height of the model domain. Stratification effects were also included through gravity terms. Perturbation pressures and temperatures were used to reduce errors. Fluxes were replaced by flux gradient transport expressions using total turbulent kinetic energy solved by a transport equation and a mixing length relation for eddy size.

A specific area in Finkenbach valley, Germany, was simulated and compared to field measurements. Effects of surface vegetation were included through two parameters; (i) the leaf surface area density and (i) a drag coefficient caused by leaves, stems and branches. Finkenbach valley trees are conifers mostly about 20 m tall. A drag coefficient $c_d = 0.2\, n_c^2$ was used where n_c is the fraction of area covered with trees. The author compared the current situation with complete deforestation. Computed results showed that when one compares points that were already deforested before and afterwards the surface temperature are very similar, but when a region was covered by trees before deforestation, then at night surface temperatures are significantly lowered whereas temperatures aloft may increase. After deforestation calculated

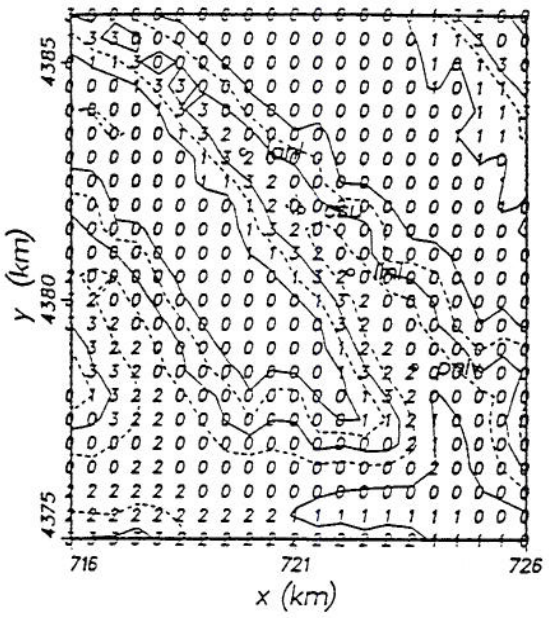

Figure 5.3.1 Distribution of tree canopies. Units are in decimal, *i.e.*, 3 indicates 0.3, 2 for 0.2, and 0 for no trees. (Yamada and Bunker, 1989)

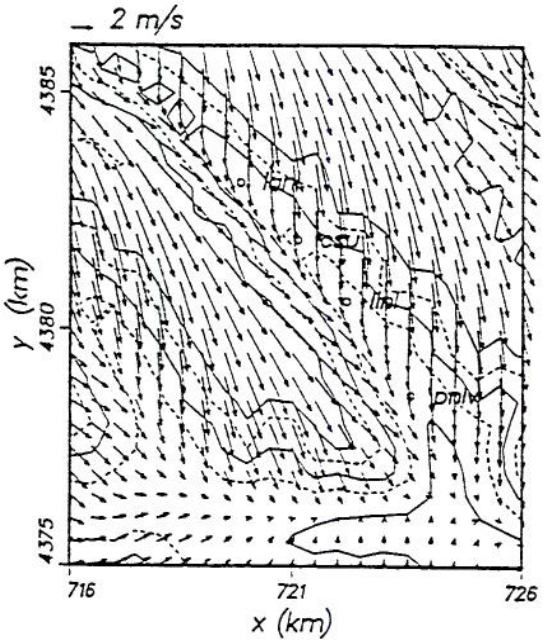

Figure 5.3.2 HOTMAC modeling of horizontal wind vectors at z = 24 m at 0200 LST. (Yamada and Bunker, 1989)

drainage winds were more intense, and the surface jet lies closer to the ground, **Figure 5.3.3.** Gross concluded after deforestation wind speed near the ground increases, depth of drainage flow decreases, surface temperatures decrease, but air aloft warms.

5.4 Spread-sheet Predictions of Wind Effects of Clearcutting

The linear-perturbation theory approach to predict effects of sudden roughness changes of airflow over 2-dimensional hills can be reduced to a few simple algebraic algorithms. These equations can be used to estimate the effect of forest clearcutting on ridge crest winds. These equations have been incorporated into a LOTUS spreadsheet, and the resultant predictions are discussed below.

5.4.1 *Linear-perturbation Expressions for Combined Changes in Roughness and Elevation*

As noted in Section 3.5.1: *Change of Roughness Models*, Jensen (1978) proposed that perturbations in mean wind velocities induced by surface roughness change could be calculated from:

$$Du(z)_{roughness} = (u_{*1}/j)\ \ln[z_{o2}/z_{o1}]\{(\ln[z/z_{o2}]/\ln[l_{zr}/z_{o2}]) - 1\}, \qquad [5.4.1]$$

where $l_{zr}\ln[l_{zr}/z_{o1}] = 2\,j^2\,x.$ [5.4.2]

Jensen and Petersen (1978) recommended perturbations induced by surface elevation change for triangular shaped hills could be calculated from:

$$Du(z)_{hill} = (u_{*1}/j)\ [1 + (h_{hill}/L)(\ln[L/z_{o1}]/\ln[l_{zh}/z_{o1}])^2]\ \ln[z/z_{o1}], \qquad [5.4.3]$$

where $l_{zh}\ln[l_{zh}/z_{o1}] = 2\,j^2\,L$ [5.4.4]

Since the solutions are separately linear their perturbations should be additive; thus

$$u(z)_{hill\ \&\ roughness} = u_o(z) + Du(z)_{roughness} + Du(z)_{hill}. \qquad [5.4.5]$$

These expressions are sufficient to calculate estimates of ridge crest wind speeds for different clearcut options over alternative slope triangular hills.

5.4.2 *Results of Spreadsheet Calculations*

Calculations were performed for a typical 300 m hill and an upwind forest with canopy height of 20 m (d = 12.6 m and z_{o1} = 3.71 m) over a range of hill slopes, (h_{hill}/L), varying from 0.05 to 1.0, clearcut to an average surface roughness, z_{o2} = 10 cm for distances upwind of the crest ranging from 0.2 L to 2 L. Data were prepared into figures that displayed resultant cresttop velocity profiles and cresttop fractional speedup factors.

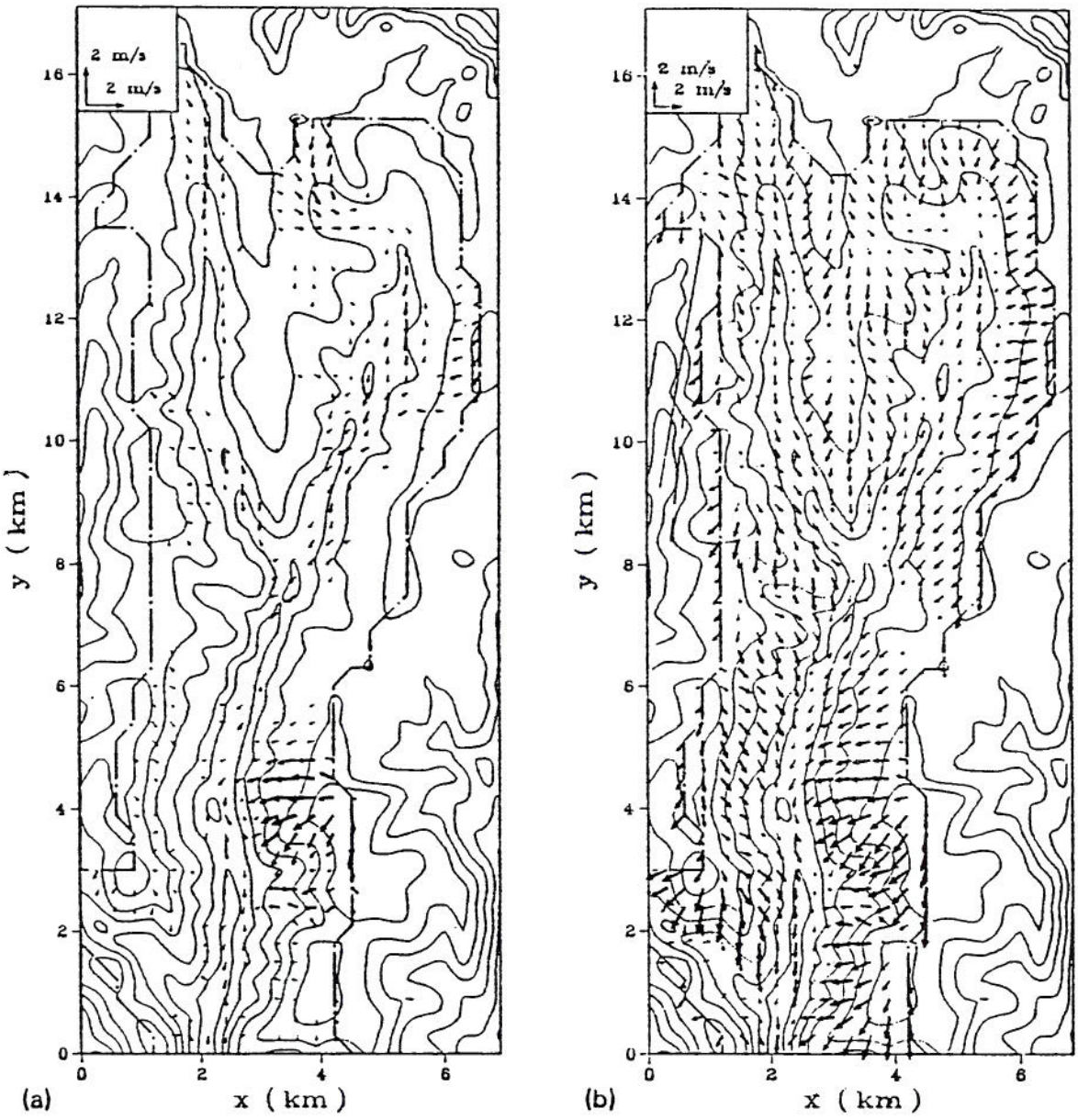

Figure 5.3.3 Computed wind vectors at 2 m above Finkenbach valley terrain: (a) with canopy, (b) after deforestation. (Gross, 1987)

Figure 5.4.1 displays inner- and outer-layer predictions of cresttop velocity profiles for a $h_{hill}/L = 0.1$ slope hill with and without clearcutting upwind to the half-height distance from the crest. Notice that the outer solution reflects the influence of the hill, but is not influenced by the change in surface roughness. Near the ground clearcutting will dominate the change in windspeed for shallow slope hills.

Figure 5.4.2 depicts the effect within the inner layer, l_z, of clearcutting upwind to the hill half-height, $x = L$, for various hill slopes. The relative improvement in windspeed decreases as hill slope increases. Since the maximum perturbation produced by roughness occurs at the ground level, the effects of tree removal on cresttop winds are most noticeable at the surface.

Figures 5.4.3 to 5.4.5 show the influence of clearcutting different distance upwind of hills with slopes, h_{hill}/L, ranging from 0.1 to 0.4. Since the inner-boundary-layer for the roughness change, l_{zr}, is now different than the characteristic inner-boundary-layer depth due to change in hill elevation, l_{zh}, the resultant wind profiles exhibit kinks where the effects of roughness and hill elevation on wind profile intersect.

Figures 5.4.6 to 5.4.8 show the same effects as **Figures 5.4.3 to 5.4.5**, but in this case the upstream roughness which characterizes the 20 m tall trees has been reduced to $z_{o1} = 1.85$ m. This roughness reflects the difference caused by using a different roughness height algorithm proposed by Lin et al. (1985) as opposed to the roughness algorithm proposed by Jaeger (1985).

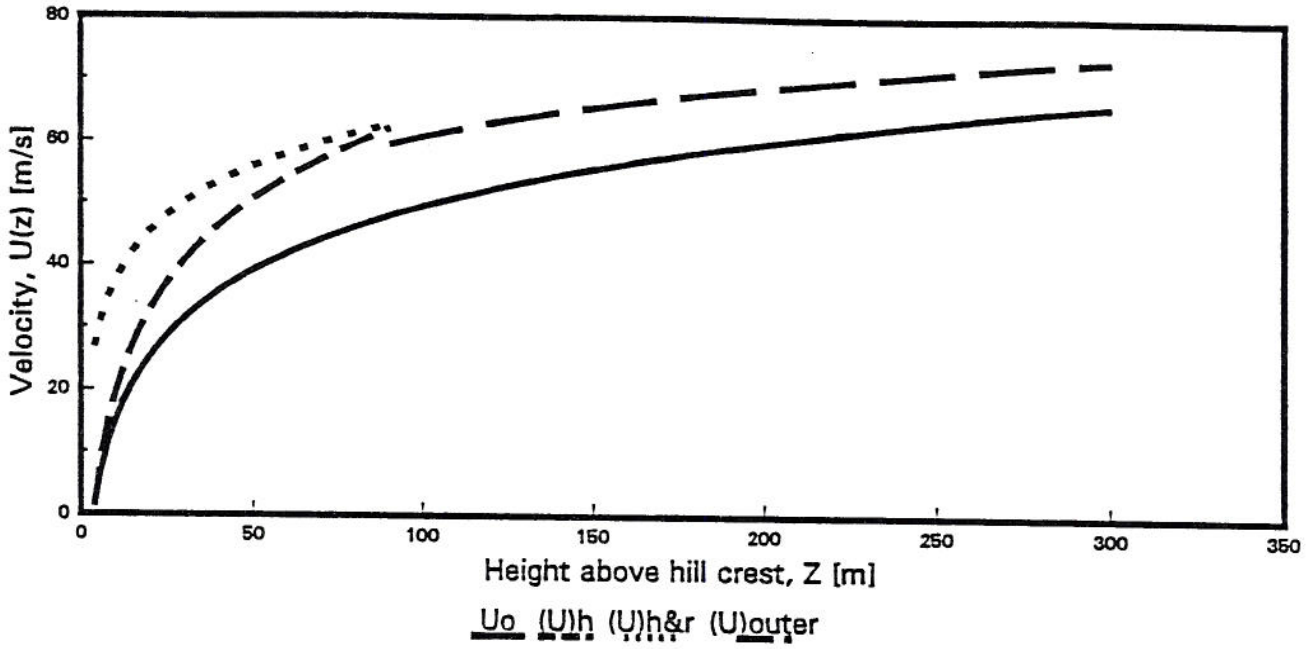

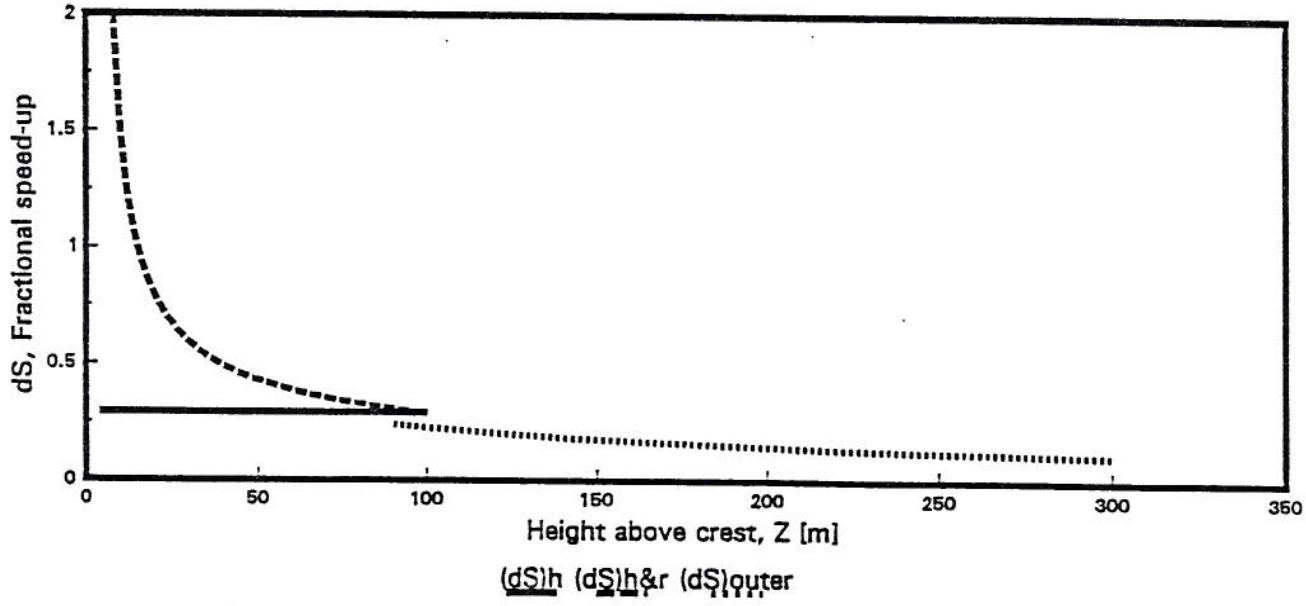

Figure 5.4.1 Linear-perturbation. Inverse-polynomial hill. h_{hill} = 100 m, L = 1000 m, z_{o1} = 3.71 m, z_{o2} = 0.1 m. U_{10m} = 10 m/s.

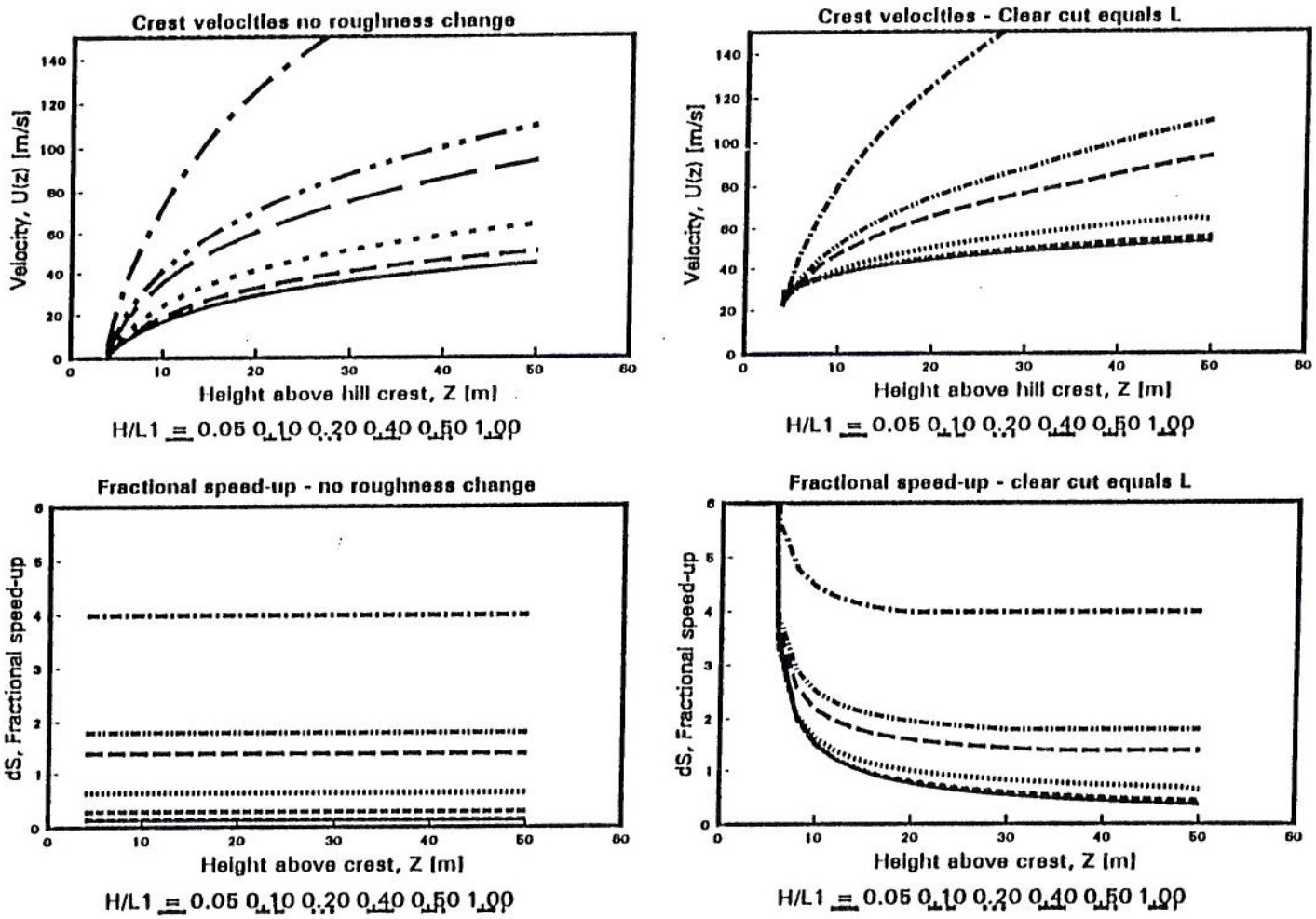

Figure 5.4.2 Effects of clearcutting upwind to the hill half-height, h_{hill} /L = L for various hill slopes. z_{ol} = 3.71 m.

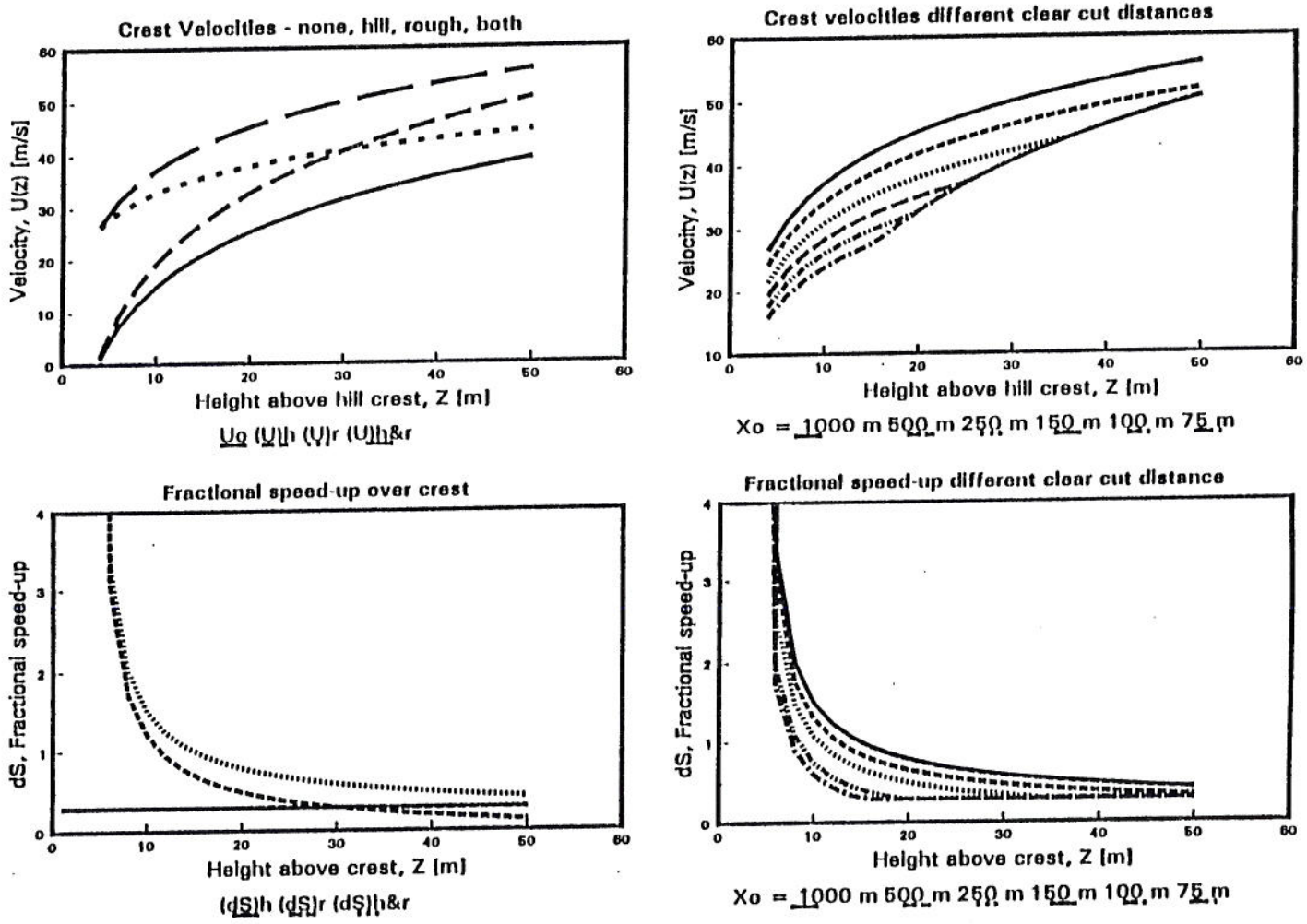

Figure 5.4.3 Influence on windspeed of clearcutting different distances upwind for a hill slope $h_{hill}/L = 0.10$. $z_{ol} = 3.71$ m.

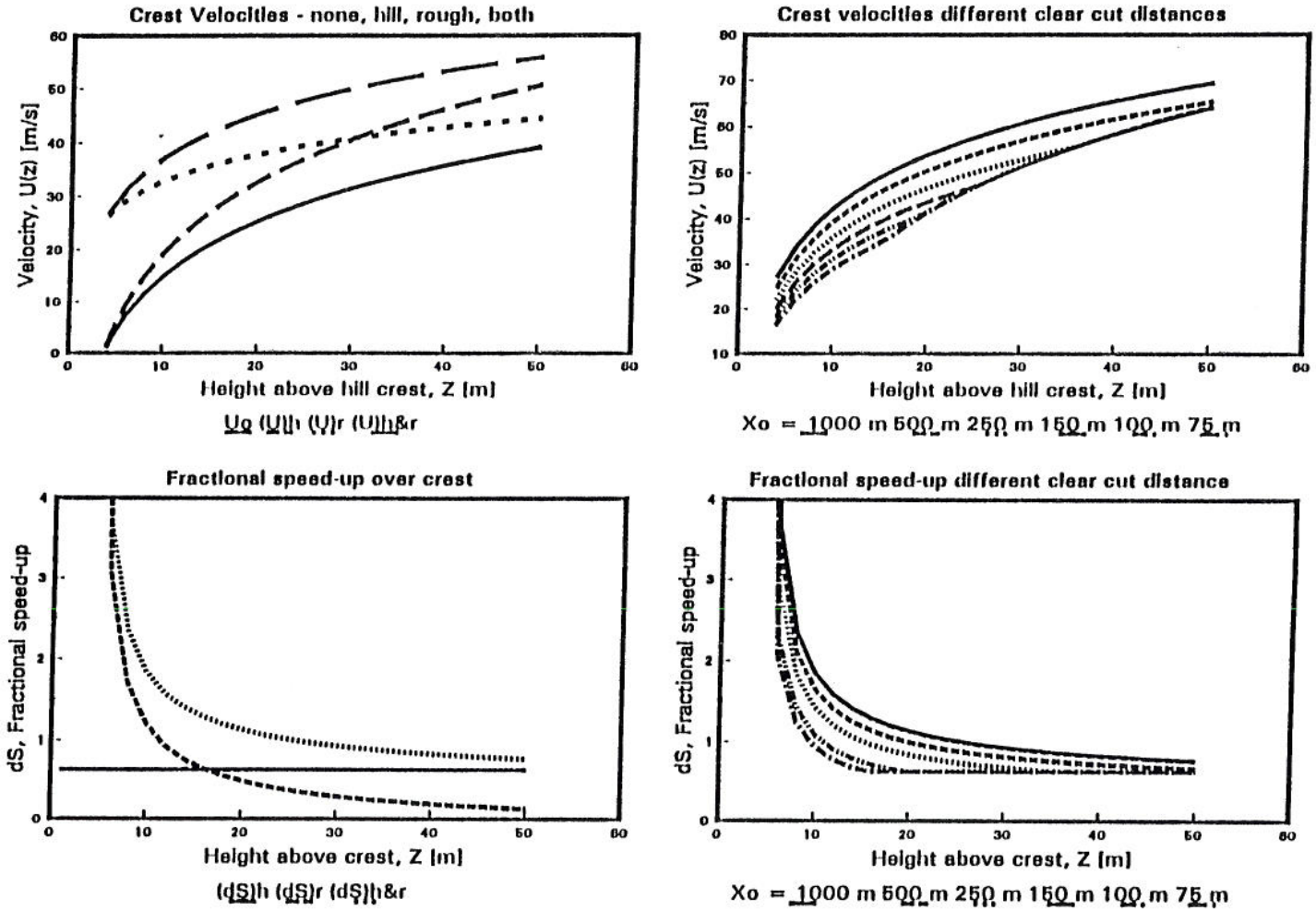

Figure 5.4.4 Influence on wind speed of clearcutting different distances upwind for a hill slope h_{hill} /L = 0.20. z_{ol} = 3.71 m.

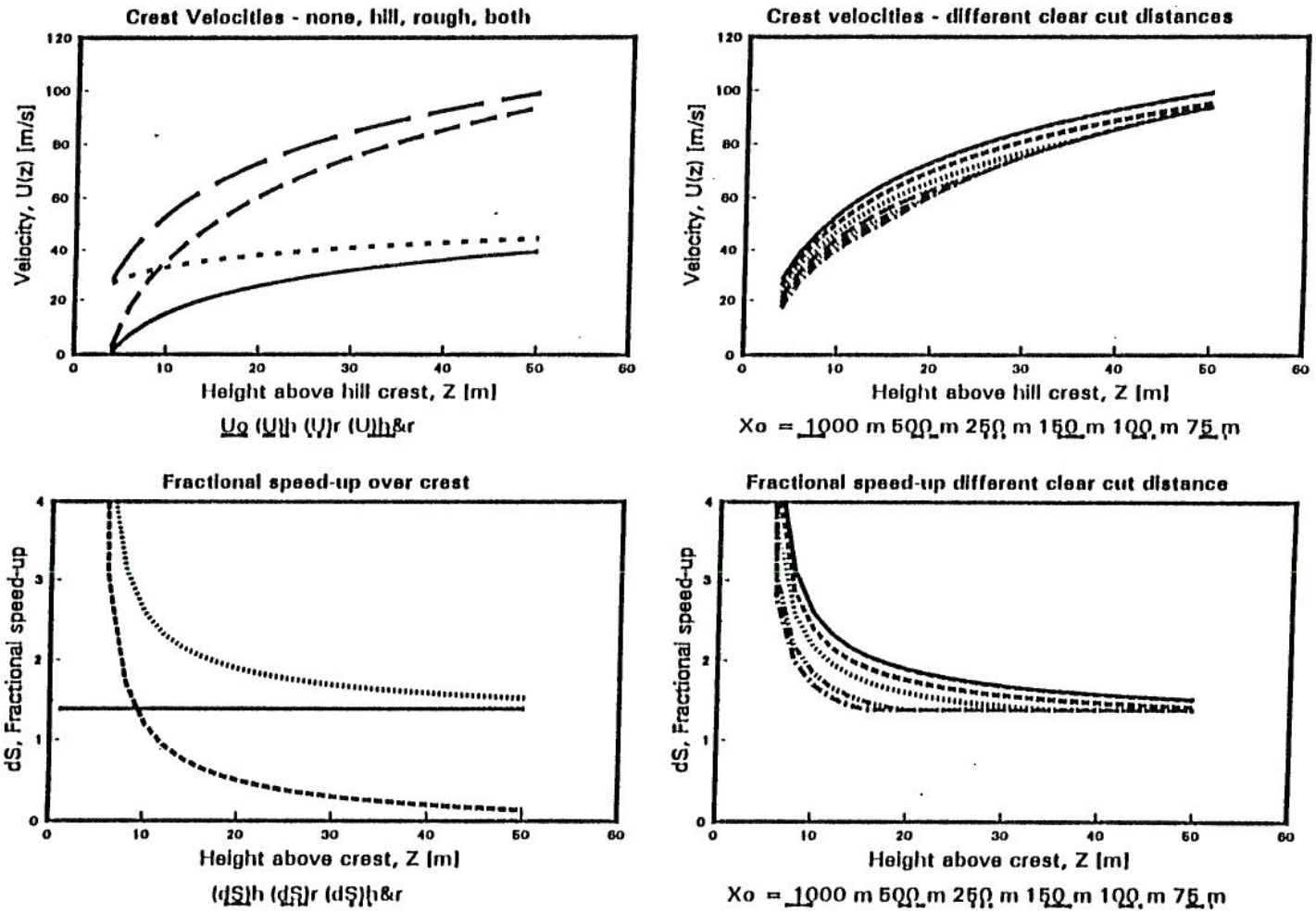

Figure 5.4.5 Influence on windspeed of clearcutting different distances upwind for a hill slope h_{hill} /L = 0.40. z_{ol} = 3.71 m.

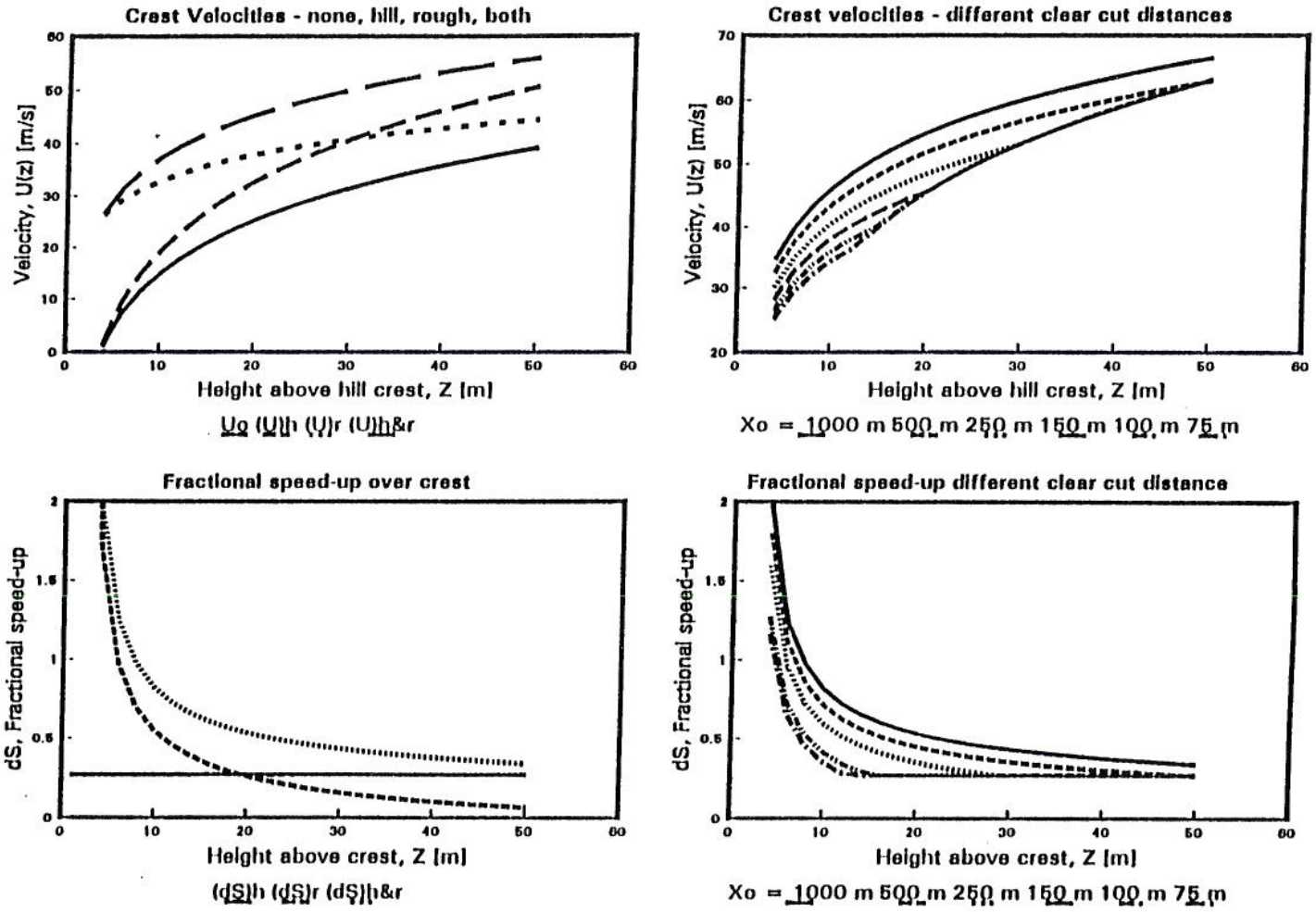

Figure 5.4.6 Influence on windspeed of clearcutting various distances upwind for hill slope h_{hill} /L = 0.10, z_{ol} = 1.85 m.

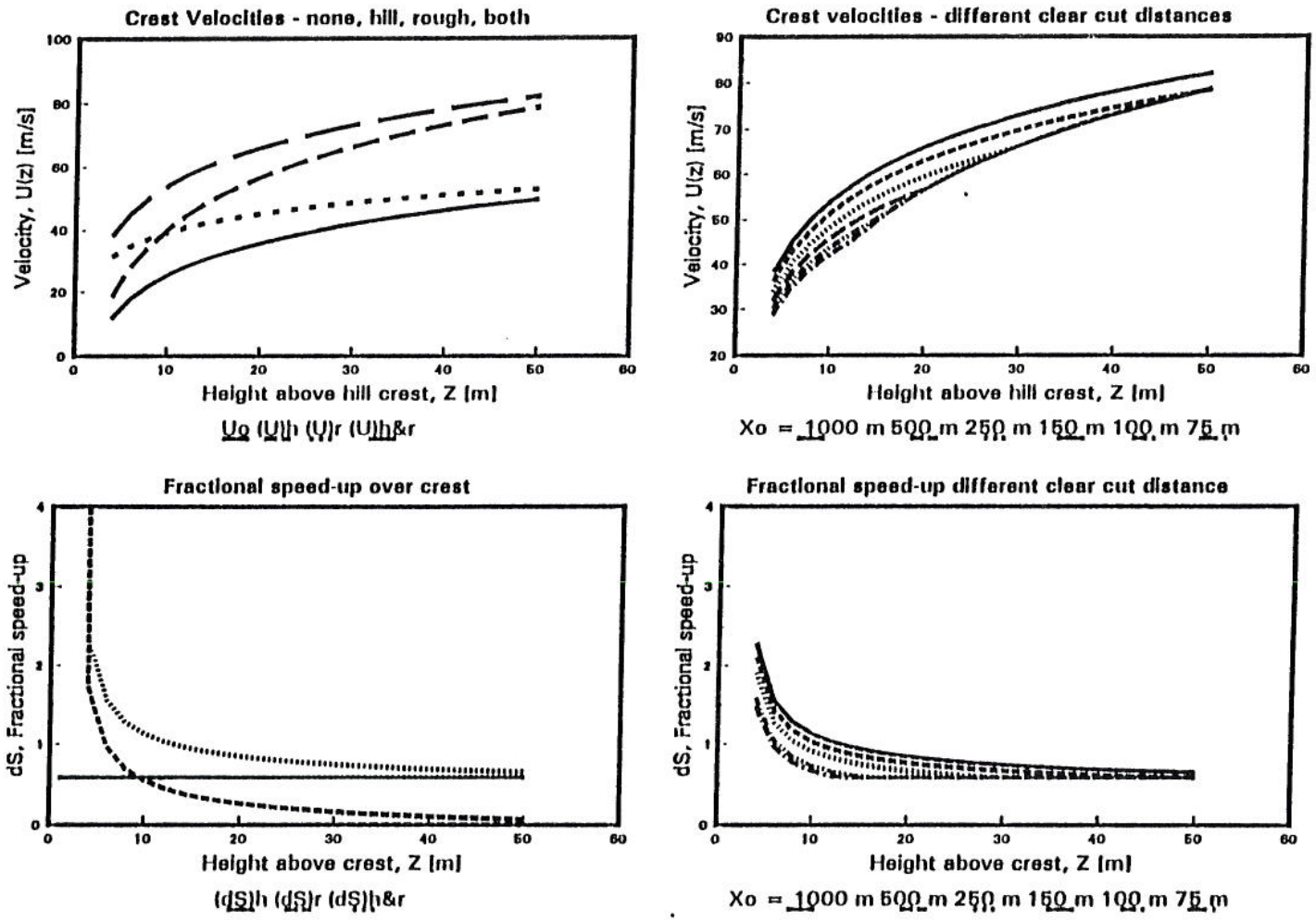

Figure 5.4.7 Influence on windspeed of clearcutting different distances upwind for hill slope h_{hill} /L = 0.20, z_{ol} = 1.85 m.